SINTEF
PROCEEDINGS
2

Proceedings of the 12th International Conference on Computational Fluid Dynamics in the Oil & Gas, Metallurgical and Process Industries

Progress in Applied CFD – CFD2017

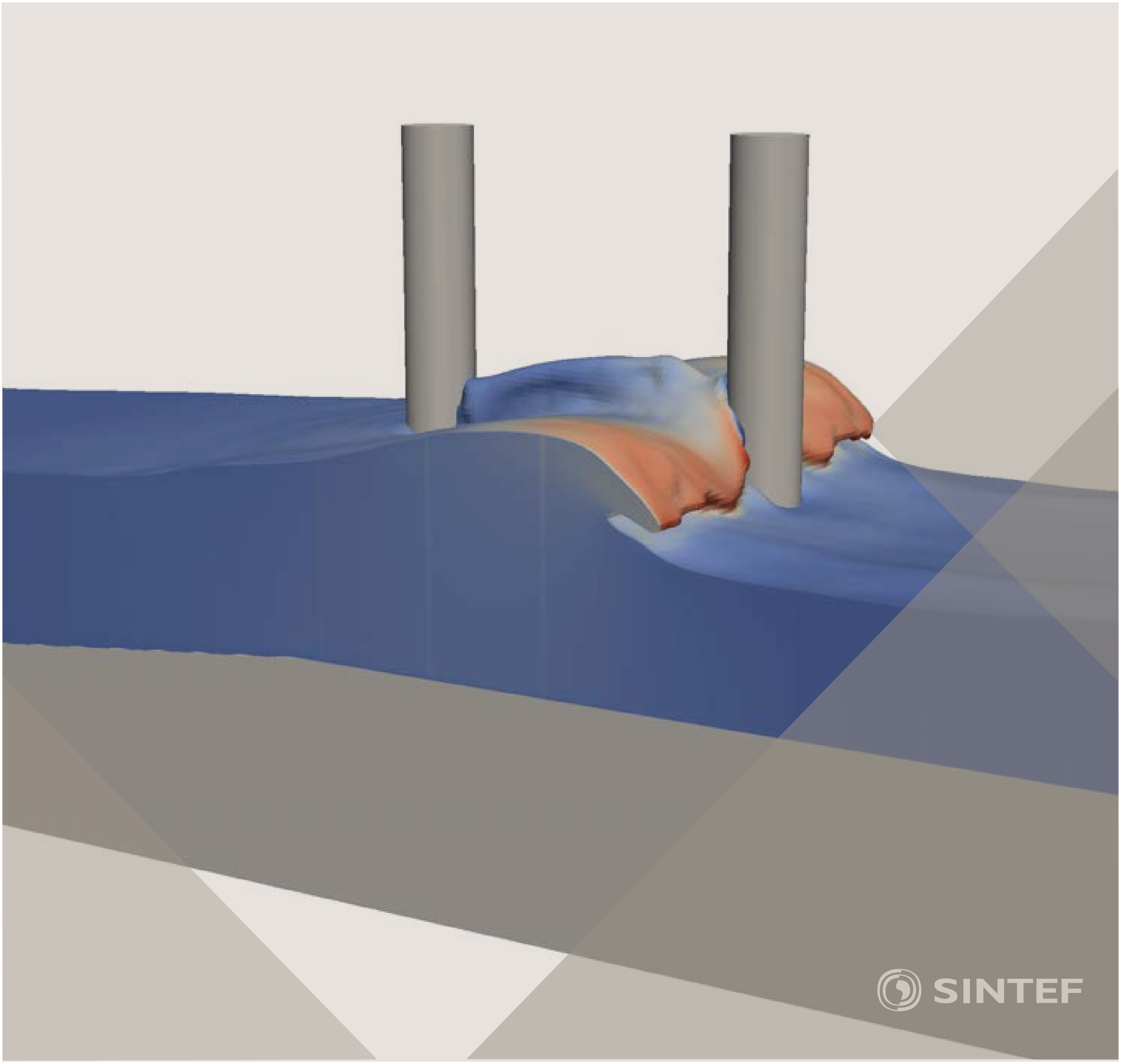

SINTEF Proceedings

Editors:
Jan Erik Olsen and Stein Tore Johansen

Progress in Applied CFD – CFD2017

Proceedings of the 12th International Conference on Computational Fluid Dynamics in the Oil & Gas, Metallurgical and Process Industries

SINTEF Academic Press

SINTEF Proceedings no 2
Editors: Jan Erik Olsen and Stein Tore Johansen

Progress in Applied CFD – CFD2017

Selected papers from 10th International Conference on Computational Fluid Dynamics in the Oil & Gas, Metallurgical and Process Industries

Key words:
CFD, Flow, Modelling

Cover, illustration: Arun Kamath

ISSN 2387-4295 (online)
ISBN 978-82-536-1544-8 (pdf)

SINTEF Academic Press

Address:	Forskningsveien 3 B
	PO Box 124 Blindern
	N-0314 OSLO
Tel:	+47 73 59 30 00
Fax:	+47 22 96 55 08

www.sintef.no/byggforsk
www.sintefbok.no

SINTEF Proceedings

SINTEF Proceedings is a serial publication for peer-reviewed conference proceedings on a variety of scientific topics.

The processes of peer-reviewing of papers published in SINTEF Proceedings are administered by the conference organizers and proceedings editors. Detailed procedures will vary according to custom and practice in each scientific community.

A CARTESIAN CUT-CELL METHOD, BASED ON FORMAL VOLUME AVERAGING OF MASS, MOMENTUM EQUATIONS

Son Tung DANG[2,*] , Stein T. JOHANSEN[1,2] , Ernst Arne MEESE[1]
[1] SINTEF Materials and Chemistry, Trondheim, NORWAY
[2] Norwegian University of Science and Technology (NTNU), Trondheim, NORWAY

[*] Corresponding author, E-mail address: son.tung.dang@ntnu.no

ABSTRACT

Simulation of multiphase flows are generally treated by various classes of Eulerian methods, Lagrangian methods and various combinations of these. In the SIMCOFLOW initiative we have set out to develop a framework for simulation of multi-material flows, using an Eulerian description. A fundamental part is the application of Cartesian grids with cut cells, and with a staggered representation of the grid for velocities and scalars. The model equations are derived based on formal volume and ensemble averaging (Gray and Lee, 1977; Quintard and Whitaker, 1995; Cushman, 1982). Solid walls or moving solid materials are treated in the same manner as any flowing material (fluid, deforming material). The interface is characterized by a level set or by a 3D surface. In grid cells which are cut with a large scale interface the stress acting at the cut surface can be computed based on the level set or volume fractions. The exchange of mass, energy and momentum between continuous fluids (note: walls are also considered a continuous fluid) can be estimated by wall functions in the case of coarse grids. The methods applied to the flow in a general geometry is closely related to the FAVOR method (Hirt and Sicilian, 1985), the LSSTAG method (Cheny and Botella, 2010) and the cut-cell method of (Kirkpatrick et al., 2003). In this paper we present the derived equations and applications of the method to a single phase two-dimensional flow, and where solid walls are treated as a non-moving secondary phase. Simulations are performed for flow over a cylinder in crossflow. Simulation results are compared with experiments from literature. The results are discussed and critical issues are pointed out.

Keywords: CFD, Cartesian grid, Cut-Cell, immersed boundary method, Level-set.

NOMENCLATURE

Greek Symbols

α^c cell fraction
α^f face fraction
ρ density (kg/m3)
ρ intrinsic density (kg/m3)
$\hat{\rho}$ extensive phase density (kg/m3), $\hat{\rho} = \alpha^c \rho$
τ viscous stress term (Pa)

Latin Symbols

G total external force (N/m^3)
p pressure at end of time step (Pa)
Se source term
Δt time step (s)
p' $p' = p - p^0$
n,N normal vector
V cell volume
A cell face area
Δh distance from velocity location to the wall
U velocity component
u the volume averaged velocity vector
Δ_i grid spacing

Superscripts

0 previous time step
c cell
f face
S solid
F fluid
w wall
b boundary
e eastern face
w western face
n northern face
P present cell
E eastern cell
N northern cell

INTRODUCTION

Simulating multiphase and multi-material flows are among the most challenging topics of computational fluid dynamic. It is not only because of the presence of numerous phases or materials but also due to the difficulty of interface treatment. Therefore, in order to model accurately the physical interactions between phases or materials, it is crucial to predict accurately the flow fields in the regions which are close to interfaces. In recent years, among many approaches, the immersed boundary method (IBM) is increasingly used in many applications to handle the coupling between materials such as in fluid-structure interactions (Ng et al., 2009; Schneiders et al., 2016) or two-phase flow (Lauer et al., 2012; Schwarz et al., 2016). In this method, the Cartesian grid is used for the whole domain, and where conventional numerical method can be applied for almost the entire flow field except for those cells which are near the boundary. Based on how the boundary condition on the immersed surface is imposed, the IBM may be classified into the continuous forcing method, the discrete forcing method and sharp interface method (Mittal and Iaccarino, 2005). Belonging to sharp interface method, the cut-cell finite volume approach is widely used due to the strict conservation of mass and momentum which is crucial in prediction of multiphase flows. Moreover, in this approach, the accurate local boundary condition is used to calculate fluxes across the cell face. Therefore, the cut-cell method is preferred and applied by several research groups (Bouchon et al., 2012; Cheny and Botella, 2010; Hirt and Sicilian, 1985; Kirkpatrick et al., 2003). Following the same approach, our code is designed to use a staggered grid representation and Cartesian Cut-Cell method (Kirkpatrick et al., 2003) to represent the immersed boundaries. In this paper, the continuity and momentum equations are derived by using a formal volume averaging method. In addition, the level-set function is applied to calculate the face and volume fractions.

It should be noted that we are now developing a dynamic grid structure, based on an octree representation. Hence, we will apply dynamic grid refinement in regions of interest, such at close to walls and fluid-fluid interfaces. This part will not be discussed herein as we will concentrate of the model formulations which can allow such complex simulations.

MODEL DESCRIPTION

The model equations are derived based on formal volume and ensemble averaging (Gray and Lee, 1977; Quintard and Whitaker, 1995; Cushman, 1982). The application of the formal volume averaging is not critical for this paper. An importance element is however that based on volume fractions, accurate boundary positions can be located and correct boundary conditions can be applied at internal as well as external boundaries. However, when we later extend our cut cell method to complex multiphase flows, the usefulness of formal volume averaging will become clearer. This will be presented in a companion paper at CFD2017.

Mass equations

According to the formalism (Cushman, 1982; Gray and Lee, 1977; Quintard and Whitaker, 1995) the transport equation for the mass is:

$$\frac{\partial}{\partial t}\int_{V_F}\rho dV = -\int_{S_F}\rho\mathbf{u}\cdot\mathbf{n}_F dS - \int_{A_w}\rho\left(\mathbf{u}-\mathbf{u}_I\right)\cdot\mathbf{n}_{F,w}dS \tag{1}$$

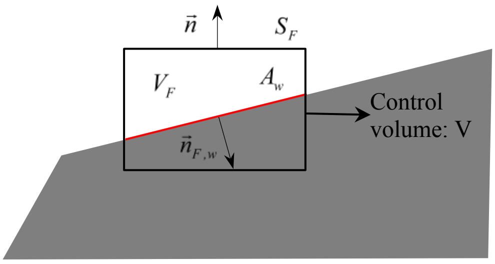

Figure 1. Control volume cut by solid

Here wall areas $A_{F,w}$, fluid volumes V_F and normal vectors $\vec{n}_F$ are explained in Figure 1. When we integrate over the fluid volume V_F we find the intrinsic average of the density. Using α_F^c as fluid fraction of the control volume the fluid mass per volume in the complete control volume is $\hat{\rho} = \alpha_F^c\rho_F = \left(1-\alpha_S^c\right)\rho_F$. Here α_S^c is the solids fraction (solid wall fraction) and $\alpha_F^c = 1-\alpha_S^c$, and where $\rho_F(p,T)$ is the intrinsic density of the fluid phase.

In Figure 2 we see a typical staggered grid layout in 2D. While the location of pressure is unchanged for both standard cell and boundary cell, the location of velocity is located at the face centre of pressure cell.

The discrete mass equation can now be represented by:

$$\begin{aligned} &\alpha_{i,j}\Delta V_{i,j}\frac{\rho_{i,j}-\rho^0_{i,j}}{\Delta t} \\ &+A_x\left(\alpha^f_{F,u}\right)_{i,j}\rho_{i+\frac{1}{2},j}u_{i,j} - A_x\left(\alpha^f_{F,u}\right)_{i-1,j}\rho_{i-\frac{1}{2},j}u_{i-1,j} \\ &+A_y\left(\alpha^f_{F,v}\right)_{i,j}\rho_{i,j+\frac{1}{2}}v_{i,j} - A_y\left(\alpha^f_{F,v}\right)_{i-1,j}\rho_{i,j-\frac{1}{2}}v_{i-1,j} = Se \end{aligned} \tag{2}$$

Where, $Se = \rho\left(\mathbf{u}-\mathbf{u}_I\right)\cdot\mathbf{n}_{F,w}.A_w$

The quantities $\alpha^f_{F,u;i,j}$ and $\alpha^f_{F,v;i,j}$ are computed from the level-set function. The simplest and first approach is:

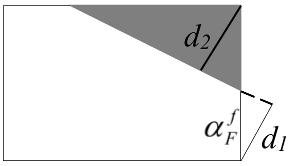

$$\alpha_F^f = \frac{d_1}{\left(d_1+d_2\right)} \tag{3}$$

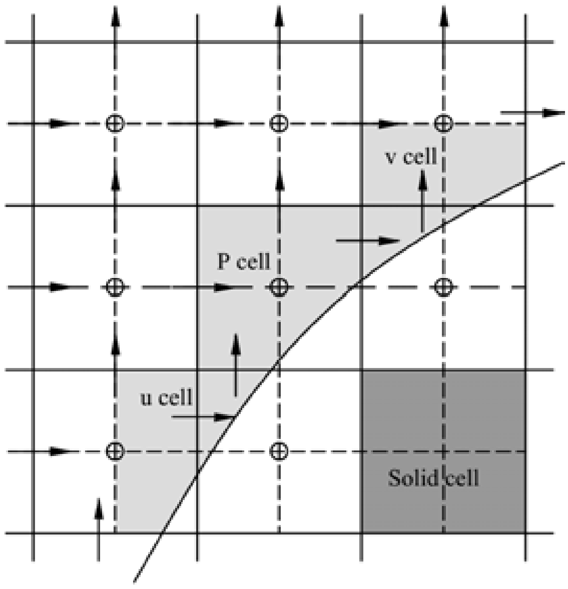

Figure 2. Staggered grid layout in 2D

Momentum equations

Similarly, the momentum equation reads:

$$\begin{aligned} \frac{\partial}{\partial t}\int_{V_F}\rho\mathbf{u}dV = \int_{V_F}\rho\mathbf{g}dV + \int_{V_F}\nabla p\mathbf{I}dV + \int_{S_F\cap A_w}\boldsymbol{\tau}\cdot\mathbf{n}_F dS - \\ \int_{S_F}\rho\mathbf{u}\mathbf{u}\cdot\mathbf{n}_F dS - \int_{A_w}\rho\mathbf{u}\left(\mathbf{u}-\mathbf{u}_I\right)\cdot\mathbf{n}_{F,w}dS \end{aligned} \tag{4}$$

The volume integrals are first evaluated, $\frac{\partial}{\partial t}\int_{V_F}\rho\mathbf{u}dV = \Delta V\frac{\partial}{\partial t}\hat{\rho}\mathbf{u}$ and $\int_{V_f}\rho\mathbf{g}dV = \Delta V\hat{\rho}\mathbf{g}$. Here the velocity and density are the volume averages, where $\hat{\rho} = \alpha_F^c\rho$. Next we do the surface integrals:

$$\Delta V \frac{\partial}{\partial t}\hat{\rho}\mathbf{u} = \Delta V \hat{\rho}\mathbf{g} - \alpha_F^c \Delta V \nabla p \mathbf{I} + \sum_{S_F} \boldsymbol{\tau}\cdot\mathbf{n}_F^f \alpha_F^f A + \boldsymbol{\tau}\cdot\mathbf{n}_{F,w} A_{F,w} - \sum_{S_F} \rho\mathbf{u}\mathbf{u}\cdot\mathbf{n}_F^f \alpha_F^f A - \int_{A_{F,w}} \rho\mathbf{u}\left(\mathbf{u}-\mathbf{u}_I\right)\cdot\mathbf{n}_{F,w} dS \qquad (5)$$

From equation (5) we see several interesting consequences:

i) The pressures gradient in term $\alpha_F^c \Delta V \nabla p \mathbf{I}$ is represented by the volume averages, which can be approximated by the difference of two adjacent pressure cell (which cell centre remains unchanged).

ii) In term $\sum_{S_F} \boldsymbol{\tau}\cdot\mathbf{n}_F^f \alpha_F^f A$, some cell faces have a zero fluid fraction ($\alpha_F^f = 0$). The contribution from these cell faces will disappear for the shear stress.

iii) The wall effect is reintroduced by the term $\boldsymbol{\tau}\cdot\mathbf{n}_{F,w} A_w$. The stress contribution will have to be computed based on the surrounding velocities.

iv) The transfer term $\int_{A_w} \rho\mathbf{u}\left(\mathbf{u}-\mathbf{u}_I\right)\cdot\mathbf{n}_{f,w} dS$ will only have values for the case where mass is entering/leaving through the wall face. In the case of an inert wall surface, moving through space, we will have zero contribution from this term. This applies to typical fluid-structure interaction cases.

Treatment of wall boundary conditions

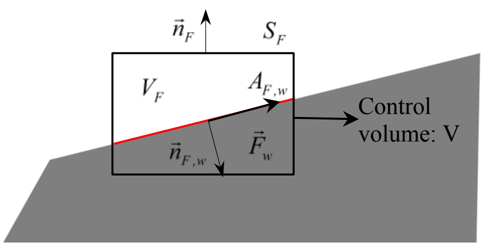

Figure 3. The force $\vec{F}_w$, acting on the fluid from the wall

In Figure 3 we see the wall shear force $\vec{F}_w$ acting on the fluid in the volume V_F. The shear force acts in the direction of the fluid velocity, tangential to the wall. The wall may have any velocity $\mathbf{u_w}$. First we need the relative velocity between the fluid and the wall, tangential to the wall. The relative velocity between fluid and wall is represented by:

$$\Delta\mathbf{U} = \mathbf{u} - \mathbf{u_w} \qquad (6)$$

The force acting on the fluid in a wall cell is now given by:

$$\vec{F}_w = -\tau_w A_w \mathbf{n_t} \qquad (7)$$

The wall force decomposed into each direction follows:

$$\begin{aligned} F_{w,x} &= -\tau_w A_w \mathbf{n_t}\cdot\mathbf{e_x} \\ F_{w,y} &= -\tau_w A_w \mathbf{n_t}\cdot\mathbf{e}_y \end{aligned} \qquad (8)$$

With

$$\begin{aligned} \tau_w \cdot \mathbf{n_t}\cdot\mathbf{e_x} &\approx \mu\frac{u-u_w}{\Delta h} \\ \tau_w \cdot \mathbf{n_t}\cdot\mathbf{e}_y &\approx \mu\frac{v-v_w}{\Delta h} \end{aligned} \qquad (9)$$

Numerical implementation

The implementation can follow the general method for doing multiphase flows. However, for simplicity we start with single phase compressible flows.

The semi discretized momentum equation for momentum in Cartesian direction i reads:

$$\begin{aligned} &\Delta V \alpha_F^c \rho \frac{U_i - U_i^0}{\Delta t} + \sum_j \left(\alpha_F^f \rho U^0 A\right)_j U_i^0 \\ &= -\alpha_F^c \Delta V \frac{\left(p_{i+1}-p_i\right)}{\Delta_i} + \sum_j \left(\tau_{ij}(U_i)\alpha_F^f A\right)_j \\ &-\tau_w(U_i) A_{F,w} n_{t,i} + \Delta V G_i^0 - \left(\rho U^0 n_{F,w}\right)_j \left(U_i - U_{w,i}\right)^0 A_{F,w} \end{aligned} \qquad (10)$$

We next do the first fractional step for the momentum equation, solving for the temporary velocity U_i^*:

$$\begin{aligned} &\Delta V \alpha_F^c \rho \frac{U_i^* - U_i^0}{\Delta t} + \sum_j \left(\alpha_F^f \rho U^0 A\right)_j U_i^0 \\ &= -\alpha_F^c \Delta V \frac{\left(p_{i+1}^0-p_i^0\right)}{\Delta_i} + \sum_j \left(\tau_{ij}(U_i^*)\alpha_F^f A\right)_j \\ &-\tau_w(U_i^*) A_{F,w} n_{t,i} + \Delta V G_i^0 - \left(\rho U^0 n_{F,w}\right)_j \left(U_i - U_{w,i}\right)^0 A_{F,w} \end{aligned} \qquad (11)$$

In this first step we solved implicitly for the viscous stresses (turbulent stresses are straight forward, can easily be included later). In next step, by subtracting equation (11) from equation (10), we obtain:

$$\begin{aligned} &\Delta V \alpha_F^c \rho \frac{U_i'}{\Delta t} = \\ &-\Delta V \alpha_F^c \frac{p_{i+1}' - p_i'}{\Delta_i} - \left(\tau_w(U_i^* + U_i') - \tau_w(U_i^*)\right) A_{F,w} + \\ &\sum_j \left\{\left(\tau_{ij}\left(U^* + U'\right) - \tau_{ij}(U^*)\right)\alpha_F^f A\right\}_j \\ &\approx -\Delta V \alpha_F^c \frac{\left(p_{j+1}' - p_j'\right)}{\Delta_j} - \mu\frac{A_w}{\Delta h} U_i' \end{aligned} \qquad (12)$$

We should note that α_F^f is the cell-face value, telling exactly the fraction of a cell face area being available for flow.

In equation (12) we have an equation for the implicit correction of the velocity. Similar to SIMPLEC method, we assume the error of neighbour cells are equal to the centre cell. However, in this case the convective momentum terms are discretized fully explicit, and formally we do not have any influence of neighbour cells as in the case of the SIMPLEC method.

Obtaining a pressure equation

The pressure equation will be based on the mass equation.

$$\Delta V \alpha_F^c \frac{\rho - \rho^0}{\Delta t} + \sum_j \left\{\rho^0 \left(U^* + U'\right)\alpha_F^f A\right\}_j = Se^* \qquad (13)$$

For incompressible flow $\rho = \rho^0$, and inserting the velocity correction from equation (12), we have:

$$-\sum_{\mathrm{j}} \left\{\rho^0 U' \alpha_F^f A\right\}_j = Se^* - \sum_{\mathrm{j}} \left\{\rho^0 U^* \alpha_F^f A\right\}_j \tag{14}$$

And where

$$U'_j = -\frac{\alpha_F^c \Delta V}{\dfrac{\alpha_F^c \Delta V \rho^0}{\Delta t} + \mu \dfrac{A_w}{\Delta h}} \frac{\left(p'_{j+1} - p'_j\right)}{\Delta_j} \tag{15}$$

We take a two dimensional example, using equations (14) and (15), and having a wall at the right boundary, as illustrated in pressure cell (i+1,j) in Figure 2. The pressure equation in a cell (i,j) with this wall configuration is represented by:

$$\begin{aligned} &-\left\{\rho^0 u' \alpha_F^f \Delta A_x\right\}^+ + \left\{\rho^0 u' \alpha_F^f \Delta A_x\right\}^- - \\ &\left\{\rho^0 v' \alpha_F^f \Delta A_y\right\}^+ - \left\{\rho^0 v' \alpha_F^f \Delta A_y\right\}^- \\ &= Se^* - \left\{\rho^0 u^* \alpha_F^f \Delta A_x\right\}^+ + \left\{\rho^0 u^* \alpha_F^f \Delta A_x\right\}^- - \\ &\left\{\rho^0 v^* \alpha_F^f \Delta A_y\right\}^+ - \left\{\rho^0 v^* \alpha_F^f \Delta A_y\right\}^- \end{aligned} \tag{16}$$

Here we have that:

$$\begin{aligned} u'^+ &= -\frac{\alpha_F^c \Delta V}{\dfrac{\alpha_F^c \Delta V \rho^0}{\Delta t} + \mu \dfrac{A_w}{\Delta h}} \frac{\left(p'_{i+1,j} - p'_{i,j}\right)}{\Delta x} \\ u'^- &= -\frac{\alpha_F^c \Delta V}{\dfrac{\alpha_F^c \Delta V \rho^0}{\Delta t} + \mu \dfrac{A_w}{\Delta h}} \frac{\left(p'_{i,j} - p'_{i-1,j}\right)}{\Delta x} \\ v'^+ &= -\frac{\alpha_F^c \Delta V}{\dfrac{\alpha_F^c \Delta V \rho^0}{\Delta t} + \mu \dfrac{A_w}{\Delta h}} \frac{\left(p'_{i,j+1} - p'_{i,j}\right)}{\Delta y} \\ v'^+ &= -\frac{\alpha_F^c \Delta V}{\dfrac{\alpha_F^c \Delta V \rho^0}{\Delta t} + \mu \dfrac{A_w}{\Delta h}} \frac{\left(p'_{i,j} - p'_{i,j-1}\right)}{\Delta y} \end{aligned} \tag{17}$$

These two equations (16) and (17) define our Poisson equation for the pressure. Once pressure is solved for we can compute the final velocities, using equation (17).

The handling of in/out-flow boundary conditions should be quite standard, and is not discussed here.

In the paper, we use a finite volume method where all fluxed across cell faces are balanced. Therefore, the cut-cell method will conserve mass, momentum and energy. In addition, the advective and diffusive fluxes across the cell face will be evaluated in the following sections.

Calculating advective flux

Based on the cut-cell method in (Kirkpatrick et al., 2003) the advective flux in the cut cell is calculated for U-momentum equation as follows:

$$\begin{aligned} F_{adv} &= \left(\alpha_F^f \rho A U^2\right)_f \quad &&\textit{for x direction} \\ F_{adv} &= \left(\alpha_F^f \rho A U V\right)_f \quad &&\textit{for y direction} \end{aligned} \tag{18}$$

Here α_F^f is the fluid fraction at the cell face and A is the area of the face. In the x direction, for the standard cell, a typical central interpolation is used to compute the velocity at the centre of cell face

$$u_e = \left[(1-\theta) u_P + \theta u_E\right] \tag{19}$$

Where, $\theta = \dfrac{\Delta x_e}{\Delta x_E}$

For boundary cell the interpolated velocity is slight off the centre of cell face as shown in Figures 4 and 5. Therefore, a modification is needed to correct the velocity at this position.

$$u_{ec} = \alpha_c \left(u_e - u_b\right) + u_b \tag{20}$$

With, $\alpha_c = \dfrac{h_{ec}}{h_e}$

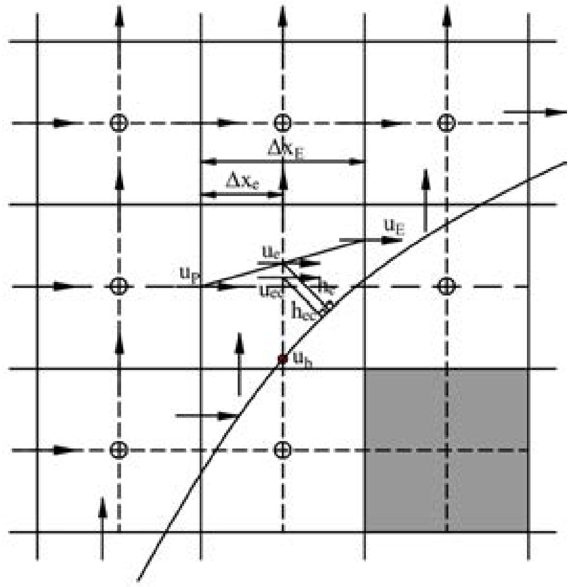

Figure 4. The schematic of interpolation and correction method for u at cell face

In y direction,

$$v_n = \left[(1-\theta_e) v_{ne} + \theta_w v_{nw}\right] \tag{21}$$

Where, $\theta_e = \dfrac{\Delta x_w}{\Delta x_{we}}$ and $\theta_w = \dfrac{\Delta x_e}{\Delta x_{we}}$

$$u_n = \left[(1-\theta) u_P + \theta u_N\right] \tag{22}$$

The correct velocity at cell centre:

$$u_{nc} = \alpha_c \left(u_n - u_b\right) + u_b \tag{23}$$

With $\alpha_c = \dfrac{h_{nc}}{h_n}$

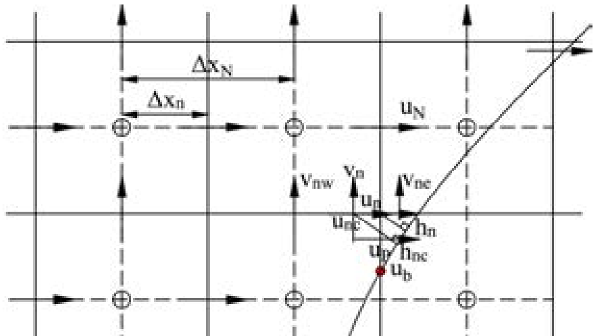

Figure 5. The location of interpolation and correction velocity at north face

Calculating diffusive flux

The diffusive flux for U-momentum equation is given as flow

$$\begin{aligned} F_{diff} &= \left(\mu \alpha_F^f \Delta A \frac{\partial u}{\partial x}\right) \quad &&\textit{for x direction} \\ F_{diff} &= \left(\mu \alpha_F^f \Delta A \frac{\partial u}{\partial y}\right) \quad &&\textit{for y direction} \end{aligned} \tag{24}$$

As seen from Figure 6, the new velocity locations, making the vector connect points E and P, may not be perpendicular to the cell face. Therefore, a modification from conventional central difference is needed in order to compute the derivative $\frac{\partial u}{\partial x}$ and $\frac{\partial u}{\partial y}$ at the cell face. Taking derivative of u along the vector $\vec{S}$ gives,

$$\frac{\partial u}{\partial s} = s_x \frac{\partial u}{\partial x} + s_y \frac{\partial u}{\partial y} \tag{25}$$

Using central difference to approximate $\partial u / \partial s$ yields,

$$\frac{u_E - u_P}{S} \approx s_x \frac{\partial u}{\partial x} + s_y \frac{\partial u}{\partial y} \tag{26}$$

Therefore,

$$\frac{\partial u}{\partial x} \approx \frac{1}{s_x}\left(\frac{u_E - u_P}{S} - s_y \frac{\partial u}{\partial y}\right) \tag{27}$$

With

$$\frac{\partial u}{\partial y} \approx N_y \frac{(u_e - u_b)}{h_e} \tag{28}$$

Where, N_y is y component of normal vector $\vec{N}$ at the surface which passes through e. The velocity u_e is evaluated by the similar interpolation as was used for advective flux.

$$\frac{\partial u}{\partial x} \approx \frac{u_E - u_P}{S_x} - \left[\frac{(1-\theta)u_P + \theta u_E - u_b}{S_x h_e} S_y N_y\right] \tag{29}$$

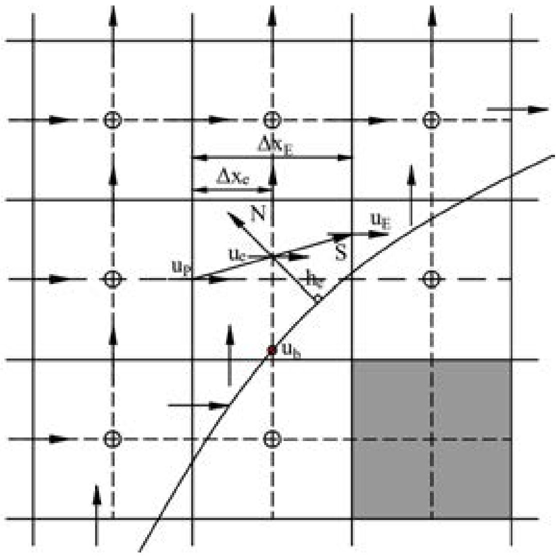

Figure 6. The vector S connects two cells and the normal vector N from the surface through the point e

Small cell problem

The presence of interface creates several velocity cells which connect to only one pressure cell. Those cells are defined as small cell (slave cell) and linked to master cell as shown in Figure 7. The detail of this method was presented in (Kirkpatrick et al., 2003).

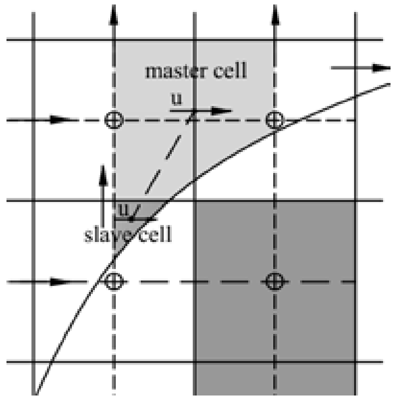

Figure 7. Linking between slave call and master cell

RESULTS AND EXTENSION TO TRUE MULTIMATERIAL FLOWS

Taylor-Couette flow

This test is performed to check the order of accuracy of the scheme. The schematic of Taylor-Couette is shown in the Figure 8. While the outer cylinder is stationary, the inner cylinder rotates with the angular velocity ω. The inside and outside radius is $R_1 = 1$ and $R_2 = 2$, respectively. The Taylor number Ta which presents characterization of the Taylor-Couette flow is defined by:

$$Ta = \frac{\omega^2 (R_1 + R_2)(R_2 - R_1)^3}{2\nu^2} \tag{30}$$

As reported by (Dou et al., 2008), the flow fields are stable with Ta smaller than 1708. According to (Cheny and Botella, 2010), the velocity fields in steady state is given as follows:

$$\begin{aligned} u(x,y) &= -K\left(\frac{R_2^2}{r^2} - 1\right)(y - y_c) \\ v(x,y) &= K\left(\frac{R_2^2}{r^2} - 1\right)(x - x_c) \end{aligned} \tag{31}$$

Where, $K = \frac{\omega R_1^2}{R_2^2 - R_1^2}$.

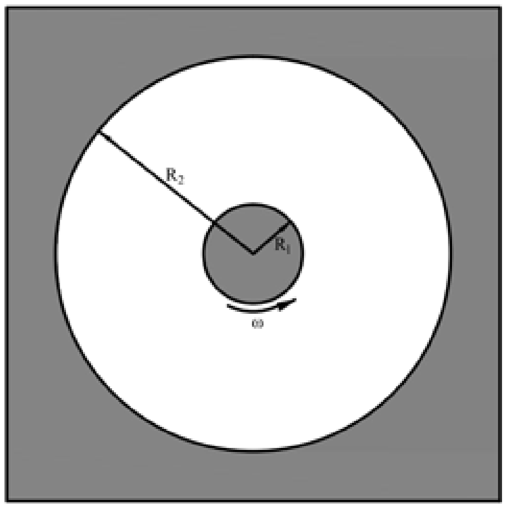

Figure 8. The geometry of Taylor-Couette flow

In this paper, the Ta is equal to 1000 and the centre of cylinder (x_c, y_c) is (0.023,0.013). The computational domain is from -5 to 5 in each direction. The grid spacing h is approximated by $1/N$, which N is grid size. The Figures 9 and 10 show the order of accuracy of the scheme for 2-norm and infinity norm. Whereas, the current method shows second order of accuracy for the 2-norm of u and v velocity, the infinity norm is slightly off from 2rd order slope.

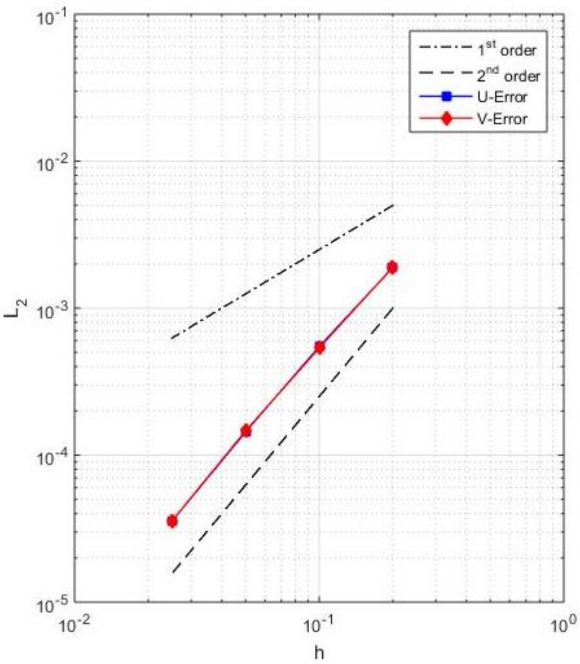

Figure 9. L2 norm of the error for velocity u and v

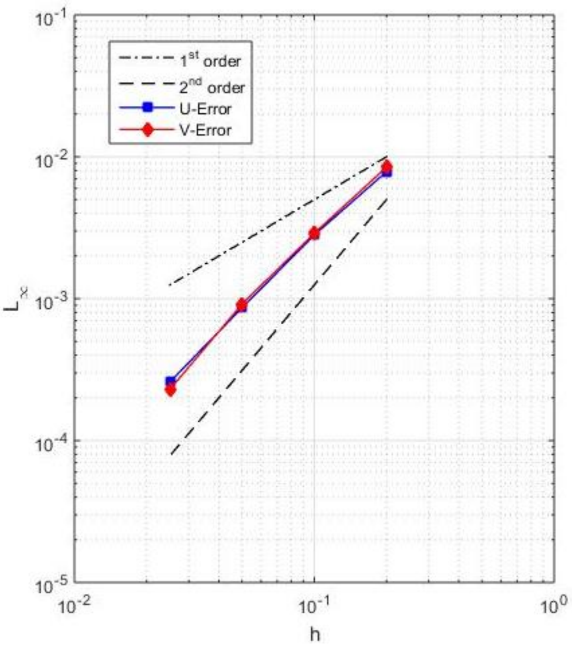

Figure 10. L∞ norm of the error for velocity u and v

Flow past a circular cylinder

Due to a significant amount of well documented test cases published in literature, the second test is the flow past a circular cylinder. The Reynolds number in this case is calculated based on the inlet velocity U_{inlet} and the diameter of cylinder D. The computational domain is illustrated in Figure 11.

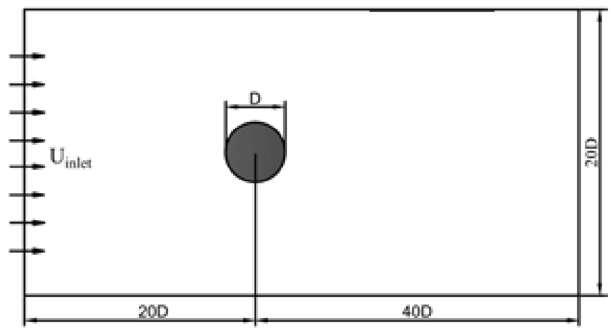

Figure 11. The computational domain

Figure 12 shows the comparison of pressure coefficient over cylinder, as obtained by present study, experiment data (Grove et al., 1964) and numerical result (Jeff Dietiker, 2009). As seen from the figure, good agreement with these reference results is observed. In addition, it can be seen that the current method can predict the pressure distribution quite accurately for coarse grids. Additional predicted properties of the flow, such as the drag coefficient, the separation angle and the size of flow separation bubble is in Table 1 seen to compare well with previous studies.

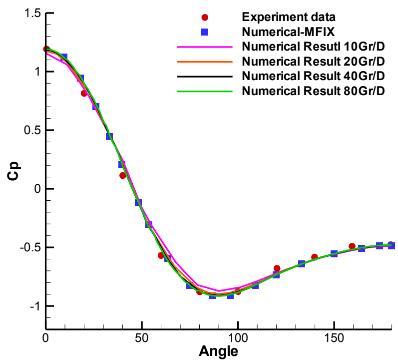

Figure 12. The pressure coefficient over cylinder at Re = 40

Re = 40	C_D	θ	L/D
Linnick and Fasel, 2005	1.54	53.6	2.28
Taira and Colonius, 2007	1.54	53.7	2.30
Kirkpatrick et al., 2003	1.535	53.5	2.26
MFIX(Jeff Dietiker, 2009)	1.542	53.7	2.27
Present Study	1.55	53.5	2.26

Table 1. The drag coefficient C_D, the separation angle θ and the length of recirculation bubble L/D behind the cylinder

Figure 13 shows the pressure contour and streamline at Re = 100. As shown in this figure, the flow became unsteady as vortex shedding formed behind cylinder. Tables 2 and 3 show that for the drag coefficient, the maximum lift coefficient and Strouhal number, our simulation results compared well with other results published in literature.

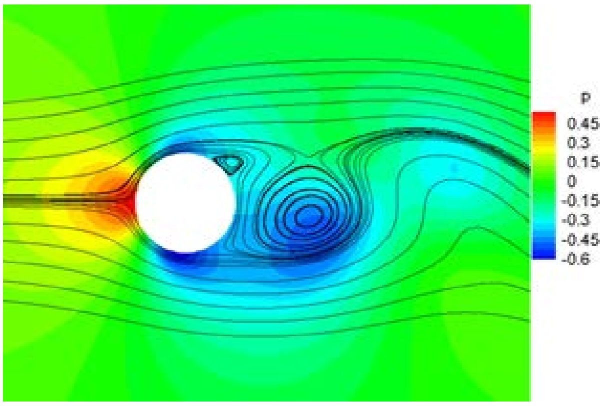

Figure 13. The pressure contour and streamline at Re = 100.

Re = 100	C_D	$C_{L,max}$	St
Linnick and Fasel, 2005	1.34±0.009	0.333	0.166
King, 2007	1.41	-	-
He et al., 2000	1.353	-	0.167
Present Study	1.374±0.01	0.337	0.169

Table 2. The Drag Coefficient C_D, the maximum Lift Coefficient $C_{L,max}$ and Strouhal number St at Re = 100

Re = 200	C_D	$C_{L,max}$	St
Linnick and Fasel, 2005	1.34±0.044	0.69	0.197
Taira and Colonius, 2007	1.35±0.048	0.68	0.196
He et al., 2000	1.356	-	0.198
Present Study	1.346±0.046	0.7	0.196

Table 3. The Drag Coefficient C_D, the maximum Lift Coefficient $C_{L,max}$ and Strouhal number St at Re = 200

CONCLUSION

A method to establish discrete transport equations for mass and momentum is presented. A semi-implicit predictor-corrector method for solving for velocities and pressure. The near interface advective flux and diffusive flux are calculated based on the interpolation technique presented by (Kirkpatrick et al., 2003). The numerical results show that our method can achieve global second order of accuracy and well predict the physical phenomena.

REFERENCES

Bouchon, F., Dubois, T., James, N., 2012. A second-order cut-cell method for the numerical simulation of 2D flows past obstacles. Comput. Fluids 65, 80–91. doi:10.1016/j.compfluid.2012.02.011

Cheny, Y., Botella, O., 2010. The LS-STAG method: A new immersed boundary/level-set method for the computation of incompressible viscous flows in complex moving geometries with good conservation properties. J. Comput. Phys. 229, 1043–1076. doi:10.1016/j.jcp.2009.10.007

Cushman, J.H., 1982. Proofs of the volume averaging theorems for multiphase flow. Adv. Water Resour. 5, 248–253.

Dou, H.-S., Khoo, B.C., Yeo, K.S., 2008. Instability of Taylor–Couette flow between concentric rotating cylinders. Int. J. Therm. Sci. 47, 1422–1435. doi:10.1016/j.ijthermalsci.2007.12.012

Gray, W.G., Lee, P.C.Y., 1977. On the theorems for local volume averaging of multiphase systems. Int. J. Multiph. Flow 3, 333–340.

Grove, A.S., Shair, F.H., Petersen, E.E., 1964. An experimental investigation of the steady separated flow past a circular cylinder. J. Fluid Mech. 19, 60–80. doi:10.1017/S0022112064000544

He, J.-W., Glowinski, R., Metcalfe, R., Nordlander, A., Periaux, J., 2000. Active Control and Drag Optimization for Flow Past a Circular Cylinder. J. Comput. Phys. 163, 83–117. doi:10.1006/jcph.2000.6556

Hirt, C.W., Sicilian, J.M., 1985. A porosity technique for the definition of obstacles in rectangular cell meshes (Flow Science Inc.). New Mexico.

Jeff Dietiker, 2009. Implementation of Cartesian Cut-Cell Technique into the Multiphase Flow Solver MFIX.

King, R. (Ed.), 2007. Active Flow Control, Notes on Numerical Fluid Mechanics and Multidisciplinary Design (NNFM). Springer Berlin Heidelberg, Berlin, Heidelberg. doi:10.1007/978-3-540-71439-2

Kirkpatrick, M.P., Armfield, S.W., Kent, J.H., 2003. A representation of curved boundaries for the solution of the Navier–Stokes equations on a staggered three-dimensional Cartesian grid. J. Comput. Phys. 184, 1–36.

Lauer, E., Hu, X.Y., Hickel, S., Adams, N.A., 2012. Numerical modelling and investigation of symmetric and asymmetric cavitation bubble dynamics. Comput. Fluids 69, 1–19. doi:10.1016/j.compfluid.2012.07.020

Linnick, M.N., Fasel, H.F., 2005. A high-order immersed interface method for simulating unsteady incompressible flows on irregular domains. J. Comput. Phys. 204, 157–192. doi:10.1016/j.jcp.2004.09.017

Ng, Y.T., Min, C., Gibou, F., 2009. An efficient fluid–solid coupling algorithm for single-phase flows. J. Comput. Phys. 228, 8807–8829. doi:10.1016/j.jcp.2009.08.032

Quintard, M., Whitaker, S., 1995. AEROSOL FILTRATION: AN ANALYSIS USING THE METHOD OF VOLUME AVERAGING. J Aerosol Sci 26, 1227–1255.

Schneiders, L., Günther, C., Meinke, M., Schröder, W., 2016. An efficient conservative cut-cell method for rigid bodies interacting with viscous compressible flows. J. Comput. Phys. 311, 62–86. doi:10.1016/j.jcp.2016.01.026

Schwarz, S., Kempe, T., Fröhlich, J., 2016. An immersed boundary method for the simulation of bubbles with varying shape. J. Comput. Phys. 315, 124–149. doi:10.1016/j.jcp.2016.01.033

Taira, K., Colonius, T., 2007. The immersed boundary method: A projection approach. J. Comput. Phys. 225, 2118–2137. doi:10.1016/j.jcp.2007.03.005